

THE ENCYCLOPEDIA OF  
**Mass Spectrometry**

Volume 1

Theory and Ion Chemistry

Edited by

**MICHAEL L. GROSS**

*Washington University, St. Louis, USA*

**RICHARD CAPRIOLI**

*Vanderbilt University School of Medicine, Nashville, USA*

Volume Editor

**PETER B. ARMENTROUT**

*University of Utah, Salt Lake City, USA*



**ELSEVIER**

AMSTERDAM – BOSTON – HEIDELBERG – LONDON – NEW YORK – OXFORD  
PARIS – SAN DIEGO – SAN FRANCISCO – SINGAPORE – SYDNEY – TOKYO

- (23) Glenewinkel-Meyer, T.; Gerlich, D. Single and Merged Beam Studies of the Reaction  $\text{H}_2^+ + \text{H}_2 \rightarrow \text{H}_3^+ + \text{H}$ . *Israel J. Chem.* **1997**, *37*, 343–352.

W. R. Gentry

University of Minnesota, Minneapolis, Minnesota,  
USA

## RF Ion Guides

### 1. Introduction

Over the last few decades the interest in the experimental investigation of the detailed dynamics of collision processes has resulted in the construction of a variety of novel devices. For many years, studies of ion–molecule reactions in the range of chemical energies were dominated by swarm and trapping techniques yielding predominantly thermal reaction rate coefficients, whereas beam methods, which can provide detailed information on reaction dynamics, were restricted to higher energies, typically above 1 eV (see *Instrumentation: Crossed Beam Methods for Ion Collisions*). This is partly because electrostatic potentials, used in most early instruments for handling charged particles, are not well suited for transferring slow ions with high transmission probability, especially if space charges and field distortions are involved.

One of the approaches to reduce these problems was to operate two beams containing the reactants with high velocities in the laboratory frame. As discussed in *Instrumentation: Merged Beams*, they can be tuned such that collisions take place at very low relative velocities. A more general solution has been found by confining slow ions via suitable effective potentials created by fast oscillatory electric fields. As discussed and illustrated in this article, this method has removed most of the inherent difficulties encountered by standard electrostatic techniques and it has revolutionized our ability to handle slow charged ions, clusters, and also nanoparticles.

On the basis of this technique, which allows one to create two- and three-dimensional potential minima, a variety of new instruments has been developed. Many of them are dedicated to the study of low-energy collision dynamics but the confinement of ions by the effective potential has also been shown to be extremely useful in photofragmentation, photoionization, and ion spectroscopy where one often needs elongated overlapping volumes between the ions and a laser beam. Moreover, many applications of radio-frequency (RF) devices can be found in commercial instruments sold for mass spectrometry and chemical analysis. Of fundamental importance for many applications is that RF ion guides allow one to compress the phase space (the position and velocity

distributions) of an ion ensemble by inelastic collisions, whereas electrostatic focusing devices are restricted by the laws of classical mechanics, e.g., the Liouville theorem. Buffer gas cooling in ion guides often significantly increases the detection sensitivity.

The principle of guiding or trapping charged particles by time-dependent forces has a longer history than its application in gas-phase ion chemistry and mass spectrometry. It was in the early 1950s that researchers in various laboratories realized that charged particles can be confined in electric fields if they alternate fast enough in time. The most prominent examples of the use of RF fields are the quadrupole mass filter and the Paul trap (see *Instrumentation: Multiquadrupoles; Instrumentation: Ion Traps*). However, those early times also saw other activities not well recognized today, such as plasma confinement in fast oscillating fields or interaction of electrons with microwave fields or electromagnetic waves. It was found that one needs oscillating voltages in the gigahertz range for electrons and fields in the RF range (megahertz) for ions. For charged microparticles, a few hertz are sufficient. Most of the early ideas have been stimulated by methods developed in accelerator physics, e.g., the strong-focusing principle, which makes use of a series of electrostatic quadrupoles alternating in space. It was realized that the equation of motion describing fast charged particles traveling through such a structure with a periodic geometry is the same for ions moving very slowly in a quadrupole field that alternates in time with an adequate repetition period.

In the following short overview the basics of the theory are given and the adiabatic approximation and the effective potential are introduced. Some technical developments are summarized more or less in chronological order. Selected experimental results are used to illustrate a variety of applications and to give some references to the newest achievements. A comprehensive overview of the technique, the theoretical background, and many applications of inhomogeneous electric RF fields can be found elsewhere (1).

### 2. Principle of the Method: Alternating Inhomogeneous Fields

#### 2.1 Motion of a Charge in an Electric Field

In order to understand the method and the limitations of the guided ion beam technique, one needs some basic theory describing the motion of a particle under the influence of a fast oscillating force. The equation

$$m\ddot{\mathbf{r}} = q\mathbf{E}_0 \cos(\Omega t) \quad (1)$$

is the classical equation of motion of a particle with mass  $m$  and charge  $q$  moving in an electric field  $\mathbf{E}_0(\mathbf{r}) \cos(\Omega t)$ , oscillating with a frequency  $\Omega$ . This differential equation can be solved exactly if the field is homogeneous, i.e., if the amplitude vector  $\mathbf{E}_0$  has the same value everywhere in space. In this case one gets immediately the solution

$$\mathbf{r}(t) = \mathbf{r}(0) - \mathbf{a} \cos(\Omega t) \quad (2)$$

with a constant amplitude  $\mathbf{a}$  given by

$$\mathbf{a} = q\mathbf{E}_0/m\Omega^2 \quad (3)$$

This situation is illustrated in the left-hand part of Fig. 1. Note that the time average  $\langle \dot{r}(t)/\dot{r}(0) \rangle$  remains constant.

If the field  $\mathbf{E}_0(\mathbf{r})$  is inhomogeneous, Eqn. (1) can no longer be solved analytically with the exception of a few special situations. In this case, computer simulations are very useful for getting insight into specific properties of certain field geometries and for testing dependences on various parameters. The right-hand part of Fig. 1 shows a situation where the field  $\mathbf{E}_0(\mathbf{r})$  decreases with increasing  $r$  as indicated schematically by the equipotential lines. It is obvious that the resulting trajectory deviates slightly from the homogeneous case. The amplitude of the oscillatory part is almost the same, but the mean value  $r(t)$  is slowly increasing. This can be explained qualitatively by the fact that the charge experiences different fields during its oscillatory motion resulting in a slow drift towards regions of weaker fields.

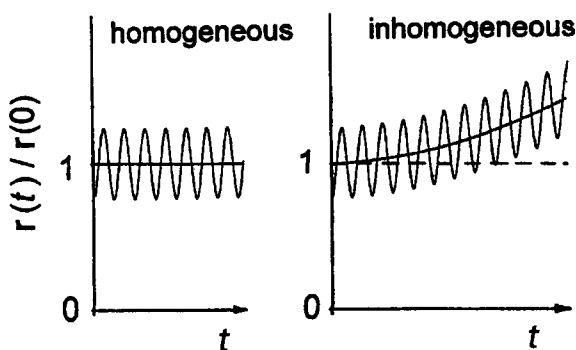


**Figure 1**

Motion of a charged particle in an oscillatory electric field. If the field is homogeneous (left) the particle oscillates with an amplitude  $\mathbf{a}$  given by Eqn. (3). In time average, it remains centered at  $r(t)/r(0) = 1$ . In the inhomogeneous field (right) the charged particle seems to be pushed away from the center by a force that is called "field gradient force." It is a general and important rule that charged particles are seeking regions of weaker fields.

## 2.2 Adiabatic Approximation

This observation can be derived in a more fundamental way by using an adiabatic approximation for solving Eqn. (1). For treating time-dependent problems adiabatic theories, in which fast and slow components are separated, are well established in theoretical physics and mathematics. Here, the rather simple calculation, which can be found elsewhere (1), is based on the idea that a solution of Eqn. (1) has the form of Eqn. (2), i.e., consists of an oscillatory part superimposed on a smooth drift term. The mathematical result leads to several important conclusions. One is that the field gradient force, acting on the particle as illustrated in the right-hand part of Fig. 1, can be derived from the time-independent mechanical potential  $V^*$  given by

$$V^* = q^2 E_0^2 / 4m\Omega^2 + q\Phi_s \quad (4)$$

where  $\Phi_s$  is the electrostatic potential. A derivation of the effective potential  $V^*$ , which is also called ponderomotive potential, pseudopotential, or quasipotential, can be found in Landau and Lifshitz (2). The other very important result is the adiabaticity parameter  $\eta$ , as defined by

$$\eta = 2q|\nabla E_0|/m\Omega^2 \quad (5)$$

where the symbol  $\nabla$ , represents the vector operator *dir*. This parameter allows one to estimate whether one operates the RF ion guide in the adiabatic limit. This parameter can be introduced in various ways, for example by postulating the condition given by

$$|2(a\nabla)E_0| < |E_0| \quad (6)$$

which means that the change of the field over the oscillation must be much smaller than the field itself. Experience based on experimental tests and on numerical calculations has shown that one should use operating conditions such that  $\eta < 0.3$ . In principle, this condition can always be achieved by using a high enough frequency. Note that in general both  $V^*(\mathbf{r})$  and  $\eta(\mathbf{r})$  are functions of the coordinate  $\mathbf{r}$ .

## 2.3 Modulation and Conservation of Kinetic Energy

To aid in the interpretation of experiments employing ions guided in RF fields, it is necessary to understand the time-dependent distortion of the ion kinetic energy caused by the confining RF field. As discussed in detail elsewhere (1), the system behaves like a conservative one on average if the conditions for the adiabatic approximation are fulfilled. This means that the ion always has almost the same kinetic energy when it moves in weak field regions. However, the momentary kinetic energy of an ion oscillates during its reflection from the RF wall.

Depending on the initial conditions, it can reach up to three times the initial energy for short times. This and also the influence of collisions with neutral molecules have been treated in much detail previously (1) using numerical simulations. For studying collision processes between neutrals and ions confined in RF fields, electrode structures leading to wide field-free regions are desirable in order to reduce the influence of the energy modulation. Note that for linear ion guides only the transverse velocity component is affected by the RF field while the main velocity component of the guided ion beam (that parallel to the symmetry axis of the guide) remains unaffected.

#### 2.4 Multipole Fields

In a real experimental device, the electric field  $\mathbf{E}_0(\mathbf{r})$  is determined by the boundary conditions imposed by suitable electrodes. For guiding and trapping ions a variety of electrode arrangements have been developed (1). The best-characterized examples are linear multipoles, which are used in many applications. Their ideal potential is given by

$$\Phi(r, \varphi) = \Phi_0 \hat{r}^n \cos n\varphi \quad (7)$$

where  $\Phi_0 = U_0 - V_0 \cos \Omega t$  is the applied potential,  $2n$  corresponds to the number of poles, and  $\hat{r} = r/r_0$  is a reduced radius. In general one operates a multipole "RF-only", i.e.  $U_0 = 0$ . From this potential one can derive the electric field

$$|E_0| = \frac{V_0}{r_0} n \hat{r}^{n-1} \quad (8)$$

With this formula, one obtains from Eqn. (4) the effective potential given by

$$V^* = \frac{1}{8} \frac{(qV_0)^2}{\varepsilon} \hat{r}^{2n-2} + qU_0 \hat{r}^n \cos n\varphi \quad (9)$$

where  $U_0$  is the applied dc potential and from Eqn. (5) the adiabaticity parameter given by

$$\eta = \frac{n-1}{n} \frac{qV_0}{\varepsilon} \hat{r}^{n-2} \quad (10)$$

It is useful for numerical calculations to introduce the characteristic energy  $\varepsilon$  defined by

$$\varepsilon = \frac{1}{2n^2} m\Omega^2 r_0^2 \quad (11)$$

using the units cm, MHz, V, the atomic mass unit  $u$ , the charge unit  $e$ , and the energy unit eV,  $\varepsilon$  can be derived from

$$\varepsilon = 1.036 \frac{1}{2n^2} m\Omega^2 r_0^2 \quad (12)$$

For  $n=2$  (a quadrupole), inspection of Eqns. (9) and (10) reveals that the effective potential  $V^*$  is harmonic and that  $\eta$  does not depend on  $\mathbf{r}$ . This leads to special properties, e.g., focusing and phase space conserving transmission (3). Moreover, the equation of motion, Eqn. (1), can be solved without approximation by transforming it into the well-known Mathieu differential equation. This allows for a mathematically precise classification of stable and unstable operating conditions. A complete theoretical description of RF quadrupoles is given by Dawson (4). Concerning the use of a quadrupole as a mass filter or as an ion guide, it must be noted that this primarily depends on the stability parameter  $\eta$  (called  $q$  in the Mathieu equation). For mass selective transmission, one operates usually with  $\eta=0.706$ , whereas for guiding ions conservation of the kinetic energy is desirable, i.e., one uses  $\eta < 0.3$ . This distinction is independent of whether one operates in the RF-only mode or with a superimposed d.c. field.

Higher-order multipoles, i.e.,  $n > 2$ , are very different from the quadrupole for a variety of reasons. Very important is that the stability parameter  $\eta$  does depend on  $r$  and goes to zero in the limit of  $r \rightarrow 0$ . This means that the adiabatic approximation is the better the closer the trajectory gets restricted to the center line. Therefore collisional relaxation is only efficient in hexa- and higher order multipoles! Another obviously important fact is that the effective potential becomes steeper with increasing  $n$ . Therefore, in many applications, the linear 22-pole guide is superior to the octopole. Some of the mentioned features of an octopole are illustrated in Fig. 2. In the inner part of the guide, the ion moves rather unperturbed on straight trajectories. If the ion comes close to a rod or approaches them in a gap, the oscillatory motion is longitudinal or transverse, respectively. The trajectory remains restricted, a consequence of the adiabatic conservation of energy. Another adiabatic constant of the motion is the orbital angular momentum of the ion motion relative to the octopole axis. For details, see Gerlich (1).

#### 2.5 Construction of Multipoles

An important question is how to construct electrodes for getting the desired electric field. In the ideal case the surfaces of the field-defining conductors have to coincide with mathematically given boundary conditions. For multipoles, the potential of which is given by Eqn. (7), this means that one should use hyperbolically shaped rods. In practice, a  $2n$ -pole device is composed of  $2n$  circular rods, equally spaced on an inscribed circle with radius  $r_0$ . To a good approximation, the diameter  $d$  of the rod can be determined from the radius of curvature of the hyperbolic potential leading to the dependence

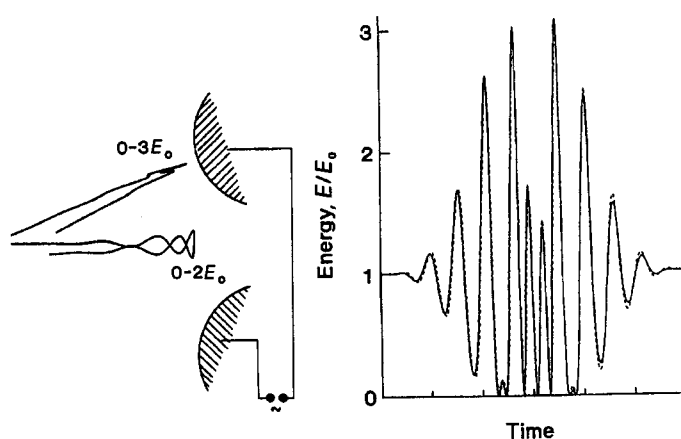


**Figure 2**

Trajectory of an ion illustrating the motion in the vicinity of two octopole rods (hatched semicircles). It can be seen that the trajectory can be composed of a smooth part  $r_0(t)$  and an oscillating part. The turning radius can be calculated from the effective potential indicating the adiabatic conservation of kinetic energy. If the ion moves towards a rod, the momentary energy is modulated between 0 and  $3E_0$ . This is shown in the right-hand part of the figure, which shows the exact ion kinetic energy as an ion approaches a rod directly (upper trajectory shown on the left).

$r_0 = (n-1)d/2$ . Typical dimensions for octopoles,  $n=4$ , are  $d=2$  mm and  $r_0=3$  mm. If one chooses  $d=1$  mm and  $r_0=5$  mm, one obtains  $n=11$ , i.e., the well-known 22 poles. For quadrupoles ( $n=2$ ), the slightly better approximation  $r_0 = (1/1.1468)d/2$  is usually used. Instead of the conventional design based on solid cylindrical rods, the boundary conditions of multipoles also have been approximated by a set of thin rods mounted on suitable hyperbolic stainless steel holders. Such a quadrupole ion guide with  $r_0=2$  cm has been described previously (3). The large radius has significantly reduced problems with surface potential distortions. Another advantage is that the transparent construction allows for efficient pumping of neutral gas.

### 2.6 How to Choose Parameters

For selecting the proper ion guide and the optimum operating parameters for a special purpose, different criteria have to be taken into account. Parameters of the multipole include the number of poles,  $2n$ , the scale length  $r_0$ , the amplitude  $V_0$ , the frequency  $\Omega = 2\pi f$ , and eventually the d.c. component  $U_0$ . The ions are characterized by the charge  $q$  and the mass  $m$ . Adiabatic conservation of energy ensures that safe transmission does not depend on the individual initial conditions, but only on the maximum transverse energy  $E_m$ . It is easy to show that a quadrupole ion guide is the best choice if one wants to confine ions

with a given  $E_m$  to a specific maximum radius  $r_m$  with a minimum amplitude  $V_0$ . From Eqns. (9) and (10) and  $\eta < 0.3$ , analytical formulas have been derived (1) that permit one to calculate "safe operating conditions." Using, for example,  $n=4$  and  $E_m=1$  eV, it is found that an amplitude  $V_0=48.8$  V is sufficient to guide a singly charged particle. This result is independent of  $m$ , i.e., it holds for electrons, protons, or heavy cluster ions. For simultaneously guiding ions with  $E_m=0.1$  eV and masses ranging from  $m_1=1$  u to  $m_2=100$  u, the values needed are  $V_0=105$  V and  $f=17.8$  MHz for an octopole ( $n=4$ ,  $r_0=0.3$  cm). It also can be shown that for a wider mass range, e.g., a factor of  $10^4$ , a decapole is preferred. More detailed examples can be found in Gerlich (1).

## 3. Guided Ion Beams: A Historical Overview

### 3.1 The 1970s

As mentioned in the introduction and as discussed in detail elsewhere (1), the use of RF fields for confining charged particles started in the 1950s. One early published experimental study in which an RF quadrupole was used to confine ions was reported by Tatarczyk and von Zahn (5). In this instrument, the decay of metastable ions was studied. The quadrupole was operated with slow enough ions that the experimental time window was in the millisecond range. The first apparatus in which an octopole was used for determining integral cross-sections for ion-molecule reactions became operational in the early 1970s (6). The term guided ion beam (GIB) technique was introduced by Henchman in an early review (7) where some of the results obtained with this first instrument were mentioned. A detailed description of this GIB apparatus and integral cross-sections for several systems have been published (8).

Figure 3 shows in detail the elements of this early instrument. An RF storage ion source was used to trap ions generated by electron bombardment and then thermalize them by buffer gas collisions. The ion source was usually operated in a pulsed mode by opening the ion gate for a few microseconds. This led to a rather high momentary peak current and allowed for time-of-flight measurements. This first octopole was made from stainless steel rods ( $d=1.4$  mm,  $r_0=2$  mm) and had a length of 24.3 cm. The effective length of the scattering cell was 8.8 cm. Because the pumping speed of the pump mounted onto this single chamber apparatus was very small ( $30$  L s $^{-1}$ ), the vacuum conductance of the cell was reduced by two tubes closely surrounding the octopole. Primary and product ions were mass analyzed by a magnetic mass spectrometer and detected using an open multiplier. Because there was no mass selection in this first version, cross-sections were measured predominantly for the rare gas ions He $^+$ , Ne $^+$ , Ar $^+$ , and for H $_3^+$  and D $_3^+$ .

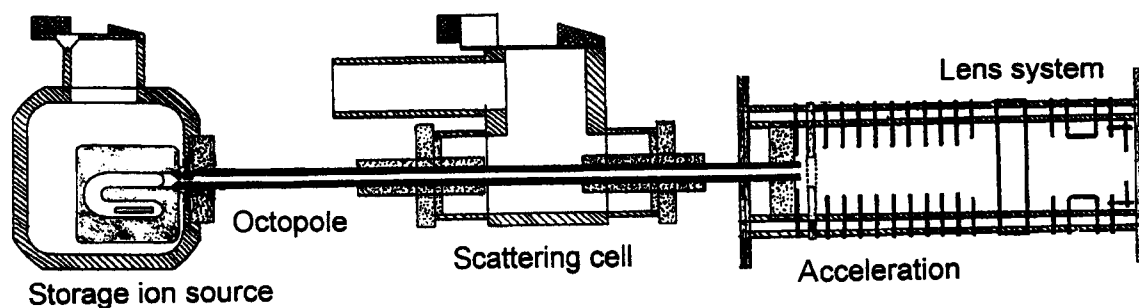


**Figure 3**

First guided ion beam apparatus; the early version of a storage ion source, the octopole surrounded by the scattering cell, and the acceleration system towards the magnetic mass spectrometer and detector (not shown). For a detailed description see Henchman (7) and Teloy and Gerlich (8) (reproduced from Diploma Thesis, University of Freiburg, 1971).

This instrument already demonstrated several outstanding capabilities of the GIB technique including a wide energy range, extreme sensitivity, and high accuracy for the determination of integral cross-sections. The cross-section for the reaction  $\text{Ar}^+ + \text{D}_2 \rightarrow \text{ArD}^+ + \text{D}$  (8) became the reference standard for comparing absolute values determined with different ion beam experiments. The reference value generally used is

$$\sigma_{\text{eff}}(E_1 = 7 \text{ eV}, T = 300 \text{ K}) = 14.5 \text{ \AA}^2$$

corresponding to an effective rate coefficient

$$k_{\text{eff}}(E_1 = 7 \text{ eV}, T = 300 \text{ K}) = 8.4 \times 10^{-10} \text{ cm}^3 \text{ s}^{-1}.$$

### 3.2 The 1980s

It took until 1979 before the second GIB apparatus became operational. In this very sophisticated instrument, the ion guiding technique was combined with molecular beams and photoionization (9). The ion source used a special ion guiding system based on a duodeca-octopole arrangement. With this apparatus the effects of both reagent translational and vibrational energy have been studied for several reaction systems.

There is no doubt that the real breakthrough of RF ion guides in ion chemistry can be attributed to two groups, one headed by Armentrout and the other one by Anderson. As nicely described in a review (10), the third guided ion beam instrument (11) was developed, among other reasons, for studying bimolecular reactions and collision-induced dissociation of ions in the threshold region (see *Thermochemistry (Methods): Reaction Threshold Energy Measurements* and *Thermochemistry (Methods): Collision-induced Dissociation*) and this method has been established as a reliable tool for getting thermochemical data. Anderson and co-workers extended the use of the GIB technique into different fields, e.g., cluster ion reactions (12) and state-specific reactions using lasers

for ion preparation (see *Ion Spectroscopy: Vibrational State Selection*).

At least three more GIB instruments have been constructed during these years. Ng and co-workers have made extensive use of photoionization coupled in various combinations with octopole beam guides and quadrupole mass filters, including a crossed ion-neutral beam photoionization instrument and a triple-quadrupole double-octopole photoionization apparatus. A convincing demonstration of the high sensitivity of the GIB technique is the "differential reactivity method" developed in this group. For a review, see Ng (13). Another new machine, combining photoionization with octopoles, became operational in Orsay, France (14). A unique aspect of this device is ion preparation using monochromatized synchrotron radiation in combination with the threshold photoelectron-photoion coincidence method (see *Ion Spectroscopy: Photoelectron Spectroscopy, Threshold Photoelectron Spectroscopy, and Pulsed Field Ionization*).

Innovative contributions to the development of the technique itself and specific applications have been briefly summarized (15) and in more detail (1). Progress has included the extension of laboratory energies below 10 meV, detection of photons from chemiluminescent reactions, and the inclusion of lasers and molecular beams. Probably the most important discovery was that the GIB technique is capable of providing information on product velocity distributions. One of the most detailed studies performed with this "universal guided ion beam machine" was on the  $\text{Ar}^+ + \text{O}_2$  charge transfer. The results included integral and differential cross-sections and also rovibrational product state distributions probed by laser-induced predissociation (16).

### 3.3 Modern Instruments

Today there are many instruments using multipole ion guides for a variety of applications. The machines

usually consist of a combination of several modules designed for ion generation and preparation (photoionization, temperature-variable traps, flow tubes, chemical ionization), methods for providing the target gas (scattering cells, molecular flows, supersonic beams), and for product detection (mass, velocity, state analyzers, chemical probing). One special ion source that makes direct use of ion guiding features and imaging properties of a quadrupole is based on multiphoton ionization of a molecular beam inside of the RF field (3).

Disregarding all these details, modern GIB arrangements usually consist of a short and a long octopole. Primary ions are injected with a defined kinetic energy into the center of the ion guide using a dedicated lens system. The first octopole, which is rather short (typically 10 cm), guides the primary ions into and through the short scattering cell (effective length is a few centimeters). The second octopole is much longer (length 50 cm or more) and is not only used to guide the reactant and product ions toward the detector but also for determining the velocity of the reaction products. The two ion guides are coupled to the same RF generator but they can be operated with a different amplitude and d.c. bias. Typically the second octopole is floated 0.1–0.5 V below the first one in order to avoid discrimination of slow ions in the transition region or resulting from potential distortions inside the second octopole. Applications can be found in the literature (17–21).

## 4. Test Procedures: A Selection

### 4.1 Transmission Function

Practical use of RF ion guides requires careful tests, e.g., the comparison of the measured transmission function with values predicted from the adiabatic theory. Some experimentally determined values for confining 20 K cold ions with  $m = 26$  u in a 22-pole ( $n = 11$ ,  $r_0 = 0.5$  cm) at  $\Omega/2\pi = 16$  MHz illustrate the situation. Partial confinement is already obtained at  $V_0 = 3$  V, whereas safe guidance requires at least  $V_0 = 10$  V. This amplitude, which corresponds to an effective potential of  $V^* = 13$  meV close to the rods, is predominantly required for compensating the surface potential distortions. Because the stability parameter is still very small,  $\eta < \eta(r_0) = 0.03$ , it is no problem to further increase  $V_0$ . Steep and highly effective potential walls created by an RF multipole have the advantage that the ions are kept further away from the perturbations caused by the conducting surfaces. In this context, it must be mentioned that the choice of the material and the treatment of the surface is very important. Best results have been obtained so far with stainless steel rods whereas gold-plated electrodes or coating with graphite was less efficient. An additional related test is the determination of the

number of transmitted ions as a function of the d.c. difference  $U_0$  applied to the electrodes.

### 4.2 Time of Flight, Energy Calibration, Oscillating Beam

Linear multipoles are ideally suited to measure the axial velocity of ions by time-of-flight (TOF) methods (see *Instrumentation: TOF and RTOF*). On the basis of a 1 m long octopole, a high-resolution velocity analyzer with unique features has been constructed (1). Because the ions are allowed to move very slowly in the ion guide, a kinetic energy resolution of better than 5 meV can be obtained, even if the time spread of the primary beam amounts to several microseconds. By accelerating the ions into the octopole, the energy range recorded within a given time window can be compressed. Deceleration, however, leads to a stretching of the timescale without a loss in ion intensity. In such applications, the main distortions result from influences caused by the RF field in the injection region.

Another related experimental test is the determination of the axial kinetic energy distribution of ions in a multipole as a function of the voltage  $U_0$  applied to the field axis of the ion guide (the d.c. bias on the multipole). One way is to determine the beam energy by using the entrance into the ion guide as a retarding field analyzer; however, the energy distribution of the ions moving in the multipole depends on several factors. Therefore TOF is the best way to get precise information. The calibration procedure, which has been described in detail previously (1), is based on the assumption that the nominal laboratory ion energy  $E_1$  linearly depends on the voltage  $U_0$  applied to the field axis of the ion guide,  $E_1 = -q(U_0 + \Delta U)$ . It is advisable to measure  $U_0$  relative to the actual ion source potential because then the correction  $\Delta U$  provides information on shifts resulting from space charge or differences in the work function.

A very important experimental tool is auxiliary ring electrodes surrounding the linear multipole. By their weak field penetration, the axial potential inside the ion guide can be raised or lowered locally, typically of the order of mV per V. They are used for diagnostic purposes, e.g., for characterizing axial potential distortions but also for selecting and trapping an meV ion beam. In the example shown in Fig. 4, the axial field inside the 35 mm long 22-pole trap can be influenced locally by five thin plates each of which has a voltage that can be controlled separately.

One application of this device is the oscillating meV ion beam, as depicted in Fig. 5. The left panel shows two typical sets of TOF data measured with various voltages  $U_{re}$  applied to the ring electrode indicated in Fig. 4. Ions are injected and extracted for detection from and to the left respectively. The end

electrode acts as a mirror and the potential barrier created by the ring electrode is semipermeable for a given energy of the trapped ion beam. Therefore, at each reflection, a small fraction of the trapped pulse of  $\text{Ar}^+$  ions leaks out towards the detector as can be seen from the sequence of peaks. Taking the flight time for one round trip and the distance of 29 mm, the kinetic energy of the trapped ion beam,  $E_1$ , can be calculated. Corresponding results are plotted in the right panel as a function of  $U_{re}$ , which has been varied between 10 V and 100 V. As can be seen from the linear fit, the resulting ion energy is proportional to the applied voltage, the factor being in this case  $0.55 \text{ meV V}^{-1}$ . An application of the method for determining rate coefficients at meV ion energies is discussed below.

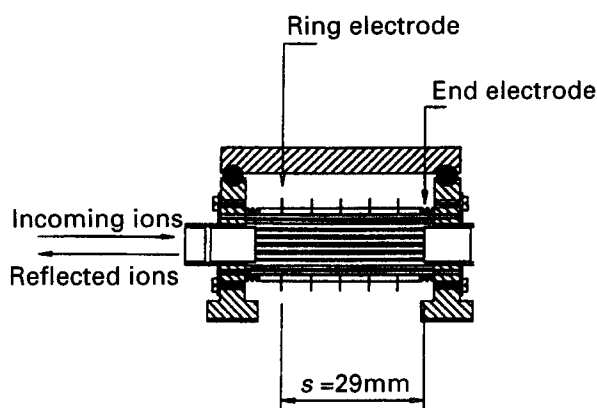


**Figure 4**  
Short 22-pole ion guide surrounded by walls (hatched regions) that can be cooled to low temperatures. This device is mainly used as a trap but also for confining slow ion beams.

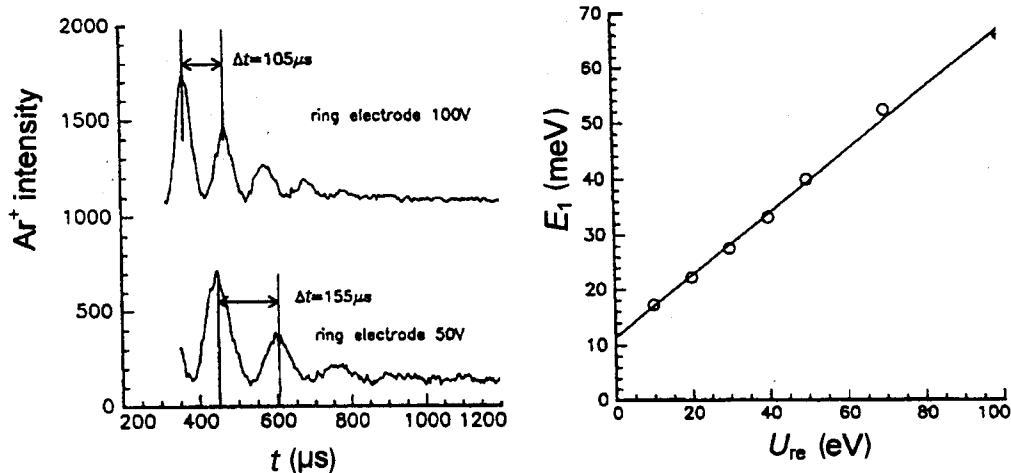


**Figure 5**  
Calibration of the kinetic energy of an  $\text{Ar}^+$  ion beam oscillating between two electrodes (see Fig. 4). The left panel shows the ion signal as a function of time for two different potentials applied to the ring electrodes. The kinetic energy, which is calculated from the distance ( $s = 29 \text{ mm}$ ) and the flight time, is plotted in the right panel as a function of the potential applied to the ring electrode.

## 5. Applications of RF Ion Guides

### 5.1 Photofragmentation in an Ion Guide

As indicated in Section 3, many versatile instruments have been constructed on the basis of RF ion guides and it is not easy to select the most typical applications from these. The progress that has been made by combining ion guiding with optical methods is discussed in the related chapters of this volume (see Chapter 4). A unique feature of RF multipoles is that not only is the primary ion beam confined but also secondary ions originating from metastable decay, produced in collisions or created by laser-induced fragmentation. The first molecular ion spectrometer in which the central element was a long RF octopole was developed by the group of Y. T. Lee. An early application of this device was to study the spin-forbidden radiative decay of metastable  $\text{O}_2^+$  (22). More applications in ion fragmentation spectroscopy are discussed in *Ion Spectroscopy: Infrared Photodissociation* and *Ion Spectroscopy: Photodissociation Spectroscopy*.

### 5.2 Thresholds and Thermochemistry

On the basis of the very large scientific output since the early 1980s, the most used feature of the GIB technique is its high precision and unprecedented sensitivity in determining integral cross-sections, especially low intensities in threshold regions. As can be seen from the historical measurement in Fig. 6, this feature was already obvious in one of the first GIB measurements (6), performed for the dissociative charge transfer reaction  $\text{Ne}^+ + \text{CO} \rightarrow \text{C}^+ + \text{O} + \text{Ne}$ .

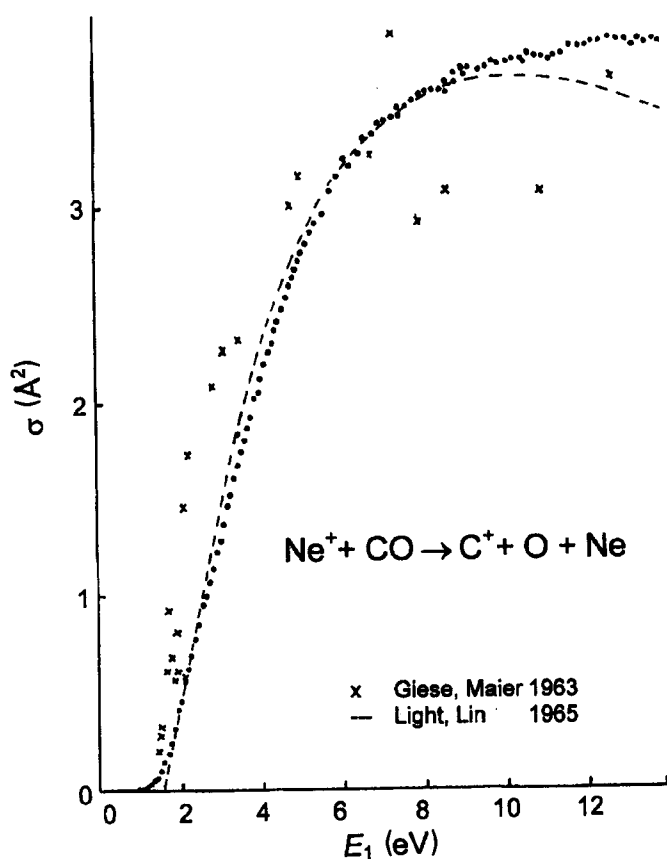


**Figure 6**  
Cross-section for the dissociative charge transfer  $\text{Ne}^+ + \text{CO} \rightarrow \text{C}^+ + \text{O} + \text{Ne}$ , measured in the threshold region. The dots are the original, uncorrected data taken from Gerlich (6); the crosses are from showing results for an early beam experiment that did not use RF ion guides; the dashed line is a phase space calculation.

It is because of the work of Armentrout that the GIB methods have become a reliable tool for determining thermochemical data. This application requires detailed understanding of the kinetic energy dependence of chemical reactions (e.g., lifetime of metastable intermediates) and the limitations imposed by the experiment (thermal motion of the target gas, internal excitation of reactants). Key contributions to this field can be found in other articles of this volume (*Thermochemistry (Methods): Reaction Threshold Energy Measurements; Thermochemistry (Methods): Collision-induced Dissociation*) and in an excellent review (10).

### 5.3 Anion Chemistry

One very fundamental recent application of a GIB apparatus was in the field of anion chemistry. From an experimental point of view, there is no difference in operating RF ion guides for positive or negative charges because the effective potential of Eqn. (4) is proportional to the square of  $q$ . One difference in a

negative system, however, is that the additional electron can give rise to reaction channels involving electron detachment. In this case, the conservation of the total number of charges, an important test for ion guides, cannot be met because the electron is not so easy to detect.

For the reactions  $\text{H}^- + \text{D}_2 \rightarrow \text{D}^- + \text{HD}$  and  $\text{D}^- + \text{H}_2 \rightarrow \text{H}^- + \text{HD}$  absolute integral and differential cross-sections have been determined in a GIB apparatus (23). Collisions of positive, neutral, or negatively charged hydrogen atoms with hydrogen molecules belong to the most fundamental molecular systems and, therefore, are interesting test cases for detailed dynamical studies. In the  $\text{H}^+ + \text{H}_2$  case, the interaction is dominated by the strongly bound  $\text{H}_3^+$  intermediate, whereas the interaction of H or  $\text{H}^-$  with  $\text{H}_2$  is predominantly determined by a barrier. From the effective cross-sections, measured in the translational energy range  $E_T = 0.1\text{--}10$  eV, thresholds for the onset of the reactions have been derived, indicating effective barrier heights of  $(350 \pm 60)$  meV for  $\text{H}^- + \text{D}_2$  and  $(330 \pm 60)$  meV for  $\text{D}^- + \text{H}_2$ . These values are substantially lower than previously reported experimental and theoretical data.

## 6. Below Thermal Energies, Towards Differential Cross-sections

For a fundamental understanding of reaction dynamics, it is important to measure state-to-state cross-sections over a wide range of collision energies and with high energy resolution. In addition, it is desirable to get information on the angular and velocity distributions of the products. In the following, improvements of ion guiding instruments by implementing molecular beams are discussed as well as the fact that not only are crossed beam arrangements (see *Instrumentation: Crossed Beam Methods for Ion Collisions*) able to obtain differential cross-sections but also RF ion guides can provide access to this type of challenging experiment.

### 6.1 Ideal Collision Experiment, Kinematics

In order to understand the principles of the GIB method and its limitations, one needs some basic knowledge in kinematic averaging (24). Typically such considerations start from an ideal scattering experiment in which two well-collimated monochromatic beams of particles with velocities  $v_1$  and  $v_2$  intersect each other. In this case, the number of products formed per unit time in the scattering volume  $d\tau$  is given by

$$dN_P = g\sigma(g)n_1n_2d\tau \quad (13)$$

where  $d\tau$  is the volume element. This equation is the definition of the intrinsic cross-section  $\sigma(g)$ . The

relative velocity is defined by  $g = |\mathbf{g}| = |\mathbf{v}_1 - \mathbf{v}_2|$  and  $n_1$  and  $n_2$  are the reacting particle densities. The corresponding intrinsic rate coefficient is defined as  $k = g\sigma(g)$ .

If one assumes that the GIB-scattering cell arrangement is ideal, i.e. (i) all guided ions move with the same velocity  $\mathbf{v}_1$  (ii) the target gas in the cell is at rest,  $\mathbf{v}_2 = 0$ , and (iii) has a homogeneous number density  $n_2$  over the cell length  $L$ , one can derive from Eq. (13) directly (1) the following:

$$N_P = N_1[1 - \exp(-n_2\sigma L)] \quad (14)$$

where  $N_1$  is the number of primary ions per second and  $N_P$  is the number of product ions per second. For weak attenuation, one can use the approximate form given by

$$\sigma = \frac{N_P}{N_1} \frac{1}{n_2 L} \quad (15)$$

In reality, the random motion of the thermal, usually 300 K, target gas causes a significant perturbation, especially a broadening of the collision energy. Moreover, the primary ion beam also has an energy spread and  $n_2$  is not homogeneous. In this case, one measures an effective cross-section  $\sigma_{\text{eff}}(\langle g \rangle)$  defined, in the limit of weak attenuation, by

$$\sigma_{\text{eff}} = \frac{N_P}{N_1} \frac{1}{\langle n_2 \rangle L} \frac{\langle v_1 \rangle}{\langle g \rangle} \quad (16)$$

where  $\langle v_1 \rangle$  is the mean velocity of the ion beam and  $\langle n_2 \rangle L$  the mean absorption length. For determining the mean relative velocity  $\langle g \rangle$ , one has to know the velocity distributions of both reactants, given by functions  $f_1(\mathbf{v}_1)$  and  $f_2(\mathbf{v}_2)$ . From these functions, one can calculate the distribution  $f(g)$  using

$$f(g)dg = \int d\mathbf{v}_1 \int d\mathbf{v}_2 f_1(\mathbf{v}_1) f_2(\mathbf{v}_2) \quad (17)$$

This function also allows one to calculate the effective cross-section  $\sigma_{\text{eff}}(g)$  from the cross-section  $\sigma(g)$

$$\sigma_{\text{eff}}(\langle g \rangle) = \int_0^\infty \frac{g}{\langle g \rangle} \sigma(g) f(g) dg \quad (18)$$

In the case of more complicated geometries, i.e., for beam-beam arrangements, the spatial overlap of the two reactants and the local densities must be known. Integration in accordance with crossed and merged beam geometries can be found elsewhere (25).

### 6.2 $\text{He}^+ + \text{O}_2$ : Collision Temperature of 33 K with 300 K Target Gas

It seems to be counterintuitive that, with a 300 K target gas, one can measure effective cross-sections at much lower temperatures. This, however, is possible

with a very slow ion beam as can be prepared by the trapped ion beam technique.

Figure 7 shows an experimental result obtained with a beam of  $\text{He}^+$  ions trapped in the region of the scattering cell of a GIB apparatus. The lower trace has been recorded by operating the electrode barrier towards the detector in the semitransparent mode. In this way, laboratory energies  $E_1$  between 10 and 100 meV can be selected (see Fig. 5). Closing the barrier and adding  $\text{O}_2$  into the scattering cell leads to a loss of  $\text{He}^+$  ions via the dissociative charge transfer  $\text{He}^+ + \text{O}_2 \rightarrow \text{O}^+ + \text{O} + \text{He}$ . In this exothermic reaction, most  $\text{O}^+$  ions formed have enough kinetic energy that they immediately surmount the exit barrier. The exponentially decreasing  $\text{O}^+$  intensity is therefore a measure for the intensity of the remaining trapped  $\text{He}^+$  ion beam. From the observed time constant,  $\tau = 2.7$  ms, and the known number density of the target gas,  $[\text{O}_2] = 6 \times 10^{11} \text{ cm}^{-3}$ , the rate coefficient for the charge transfer reaction can be derived,  $k = (\tau[\text{O}_2])^{-1}$ . In the present example, one obtains  $k = 6 \times 10^{-10} \text{ cm}^3 \text{ s}^{-1}$ . It must be noted that in this experiment  $k$  is an effective rate coefficient. As mentioned above, the collision energy distribution is determined by the ion beam energy (here  $E_1 = 60$  meV in the laboratory frame) and the temperature of the oxygen (300 K). In the limit of a very slow ion beam,  $E_1 \rightarrow 0$ , one obtains a thermal

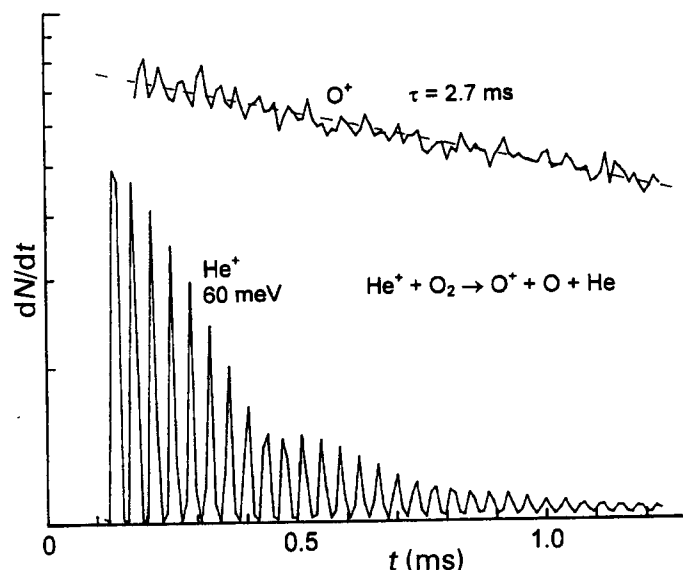


Figure 7

Experiments performed with an oscillating ion beam. A  $\text{He}^+$  ion beam, having a kinetic energy of  $E_1 = 60$  meV, is trapped in an octopole between two barriers separated by 3.2 cm. For recording the lower signal, the exit barrier was tuned such that, after each round trip, a few  $\text{He}^+$  ions leak out towards the detector. The upper curve shows  $\text{O}^+$  ions produced by dissociative charge transfer in collisions between  $\text{O}_2$  and the enclosed oscillating  $\text{He}^+$  beam.

rate coefficient at a temperature determined by the temperature of the target gas and mass ratio of the reactants. In the example, one can reach a collision temperature of 33 K ( $m_{\text{He}}/(m_{\text{He}} + m_{\text{O}_2}) = 4/36 \times 300 \text{ K}$ ) with 300 K oxygen. Note that the rotational temperature of the molecule is 300 K. Effective cross-sections measured with this method all the way down to  $\langle E_1 \rangle = 15 \text{ meV}$  can be found in Gerlich (1).

### 6.3 $\text{C}^+ + \text{H}_2$ : Gas Cell vs. Crossed Beam

In order to extend the energy range to lower energies and to obtain a better energy resolution, one can cool the scattering cell. Significant improvement, however, can only be achieved by replacing the scattering cell with a supersonic beam. For analyzing the different situations illustrated in Fig. 8 and for determining the mean collision energy  $\langle E_T \rangle$ , one has to calculate the distribution  $f(g)$  and its spread by proper averaging over the velocity distributions characteristic for a scattering cell (left), a crossed beam arrangement (center), or a merged beam arrangement (right). This can be done by numerical integration of Eqn. (17). An alternative way is indicated in *Instrumentation: Merged Beams* where the distributions are approximated by Gaussians with experimentally determined parameters.

In an arrangement where a supersonic beam crosses a GIB at right angles, one has to make sure that reactions of the ions with background gas, filling the octopole, must be less probable than with the beam itself. This only can be achieved by efficient differential pumping. So far there are only a few reactions that have been studied with the crossed GIB method (25, 26). Figure 9 compares results for the endothermic reaction  $\text{C}^+ + \text{H}_2 \rightarrow \text{CH}^+ + \text{H}$ . For forming  $\text{CH}^+$  from ground state reactants, a translational energy of  $E_T = 0.4 \text{ eV}$  is required. Note that in Fig. 11 the measured cross-sections are plotted as a function of the laboratory energy  $E_1$  for illustrating the energy shift in the methods. It is obvious that the onset of the reaction gets steeper and

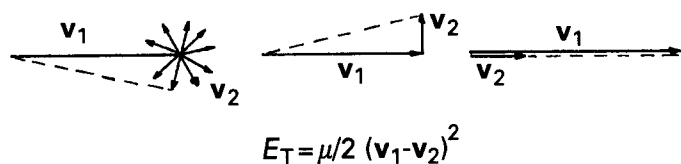


**Figure 8**  
Various kinematic situations. The translational energy,  $E_T = \mu/2(\mathbf{v}_1 - \mathbf{v}_2)^2$ , is determined by the velocities of both collision partners,  $\mathbf{v}_1$  and  $\mathbf{v}_2$ . On the left side, the ion beam interacts with target molecules in a scattering cell. In the center, the crossed beam arrangement is shown. At the right, two beams are merged, i.e., moving into the same direction.

also a larger laboratory energy is needed if one goes from the gas cell to the crossed beam target, where, for both experiments, the laboratory threshold is 2.8 eV.

### 6.4 Merged Beams

Figure 9 also shows results for the merged beam arrangement. In order to understand the very large shift of the onset, one has to evaluate quantitatively the situations illustrated in Fig. 8 using

$$E_T = \frac{1}{2} \mu g^2 = \frac{1}{2} \mu (v_1^2 + v_2^2 - 2v_1 v_2 \cos \Lambda) \quad (19)$$

where  $\mu = m_1 m_2 / (m_1 + m_2)$  is the reduced mass ( $m_1$  and  $m_2$  are the masses of the ion and the neutral, respectively). The collision energy  $E_T$  depends strongly on the angle  $\Lambda$  between the two beams. For the crossed beam arrangement,  $\Lambda = 90^\circ$ , the cosine term is zero, whereas for the merged geometry,  $\Lambda = 0^\circ$ , the ion beam energy must be larger than 5 eV for reaching the threshold. There are two remarkable consequences of using the merged beam geometry. First, discrimination effects are reduced because all products are fast in the laboratory frame. Second, the kinetic energy resolution is better, even superior to

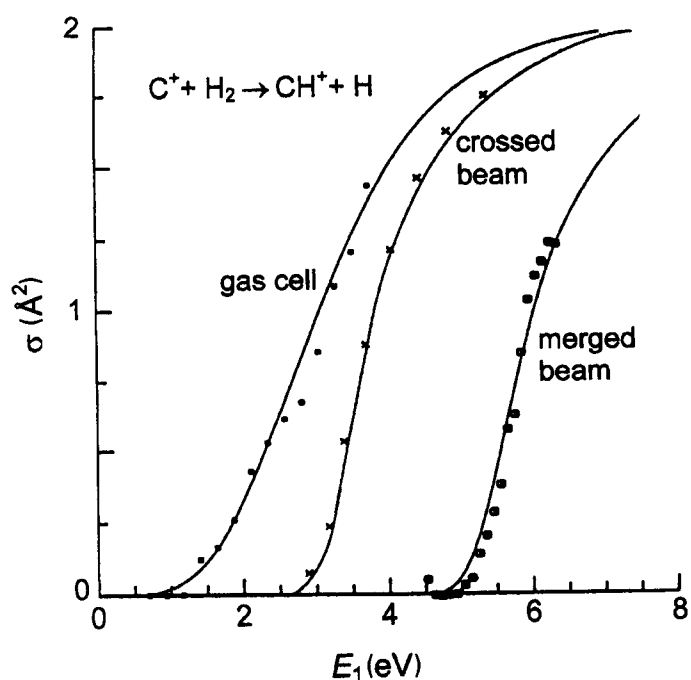


**Figure 9**  
Cross-sections for the reaction  $\text{C}^+ + \text{H}_2 \rightarrow \text{CH}^+ + \text{H}$  as a function of the laboratory kinetic energy of the guided ion beam,  $E_1$ , for the three situations depicted in Fig. 8 (gas cell, crossed beam, merged beam). The solid lines are calculated cross-sections using phase space theory and accounting appropriately for the three experimental situations.

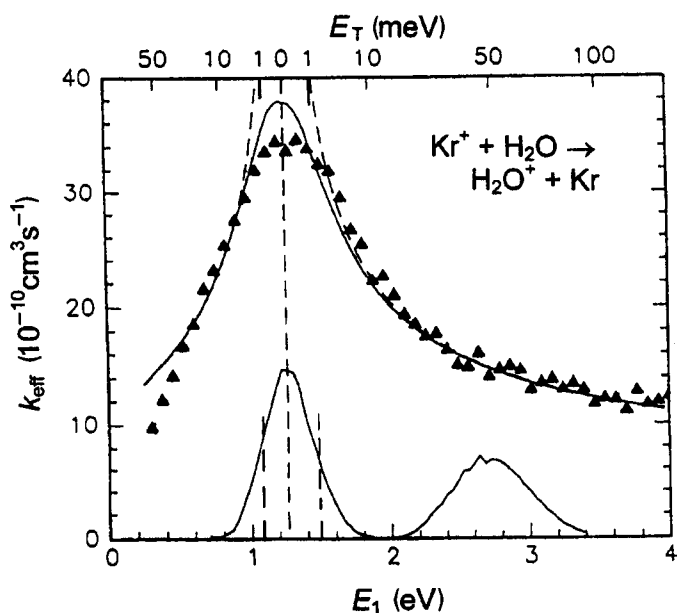


**Figure 10**

Merged beam results for the charge transfer reaction  $\text{Kr}^+ + \text{H}_2\text{O} \rightarrow \text{H}_2\text{O}^+ + \text{Kr}$ . Plotted is the effective rate coefficient  $k_{\text{eff}}$  as a function of  $E_1$ , the laboratory energy of the guided  $\text{Kr}^+$  ion beam. The  $\text{H}_2\text{O}$  beam has been seeded in He. The nominal zero point of the collision energy  $E_T$  (upper scale) is reached at  $E_1 = 1.3$  eV. The overall energy resolution can be estimated from the two distributions shown at the bottom, which have been calculated by numerical integration over the two beam spreads.

the crossed beam arrangement. In order to prove this, a simple but precise analytical estimate of the attainable energy resolution can be used, based on error propagation. For the merged beam geometry, one obtains from Eqn. (19) the expression

$$\Delta E_T = \left[ \left( \frac{\mu g}{m_1 v_1} \Delta E_1 \right)^2 + (\mu g \Delta v_2)^2 + \left( \frac{\mu}{2} v_1 v_2 \Delta \Lambda^2 \cos \Lambda \right)^2 \right]^{1/2} \quad (20)$$

where  $\Delta E_1$  is the energy half-width of the ion beam,  $\Delta v_2$  the velocity half-width of the supersonic beam, and  $\Delta \Lambda$  the mean relative angular divergence between the two beams. More details for comparing the crossed and the merged beam arrangement can be found elsewhere (25).

By combining a slow well-defined GIB with a coaxial supersonic beam, collision energies of a few meV can be reached. One of the "coldest" collisions measured with an ion beam is shown in Fig. 10. Because of the permanent dipole of the water molecule, the cross-section for exothermic charge transfer process  $\text{Kr}^+ + \text{H}_2\text{O} \rightarrow \text{H}_2\text{O}^+ + \text{Kr}$  increases

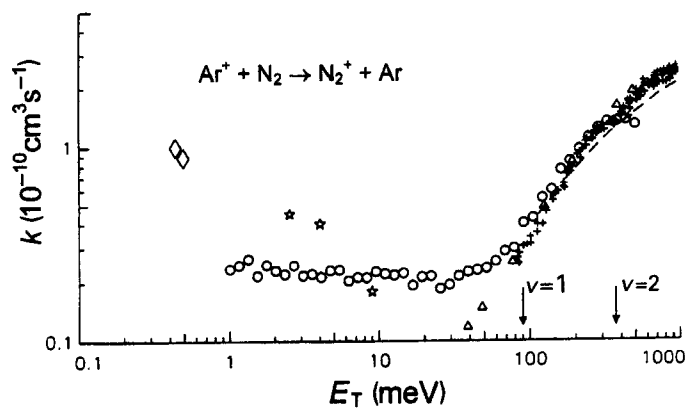


**Figure 11**

Comparison of merged beam data for the charge transfer  $\text{Ar}^+ + \text{N}_2 \rightarrow \text{N}_2^+ + \text{Ar}$  (open circles) with results measured with several other techniques: the dashed line shows results from a standard guided ion beam–collision cell experiment, the crosses are from a guided beam–crossed beam arrangement, and the diamonds and stars are from swarm experiments. The arrows indicate the thresholds for forming  $\text{N}_2^+(v)$  in the first and second vibrationally excited states.

steeply with decreasing collision energy (see *Theory (Reactions): Ion–Molecule Collision Theory*). This is emphasized in Fig. 10 by plotting the effective rate coefficient  $k_{\text{eff}}$  as a function of the laboratory energy  $E_1$  of the ion. For calculating the collision energy  $E_T$  (upper scale), one has to account for the fact that the  $\text{H}_2\text{O}$  beam has been seeded in He. Therefore the nominal zero point of the collision energy  $E_T$  is reached at  $E_1 = 1.3$  eV. The overall energy resolution has been calculated exactly by numerical integration over the angular and velocity spreads of the two beams determined experimentally. Two examples of the energy distributions are shown at the bottom of Fig. 10 by the Gaussian-like curves.

The comparison of merged beam data for the charge transfer reaction  $\text{Ar}^+ + \text{N}_2 \rightarrow \text{N}_2^+ + \text{Ar}$  with results obtained with several other techniques illustrates the wide range of collision energy that can be covered with the GIB method using a coaxial supersonic beam (circles). In Fig. 11, the dashed line above 100 meV is from a standard GIB experiment, the crosses are from a guided beam–crossed beam arrangement. The other points (diamonds and stars) are from swarm experiments.

The weakly endothermic reaction (29 meV)  $\text{N}^+ + \text{D}_2 \rightarrow \text{ND}^+ + \text{D}$  has been studied using the GIB technique combined with a crossed and a merged beam. This example, shown in Fig. 12, illustrates that, in contrast to thermal experiments, the internal excitation of the reactants and the collision energy can be varied separately. Experiments have been performed for two nozzle temperatures, 80 K and 300 K, leading to different

populations of the rotational states of the  $D_2$  molecule. For details, see Tosi *et al.* (25).

### 6.5 Differential Cross-sections

The GIB technique is best known for routinely measuring integral cross-sections at low kinetic energies, but, in contrast to what is generally believed, differential cross-sections can also be obtained (1). In general, guided ion methods allow determination of absolute doubly differential cross-sections with very high sensitivity and in an energy

and scattering angular range inaccessible to standard crossed ion beam methods. As illustrated in Fig. 13, the product velocity vector  $v_1'$  is measured by a procedure that combines TOF analysis (see *Instrumentation: TOF and RTOF*) with variation of the guiding field, leading to the component  $v_{1p}'$  parallel to the axis and the transverse component  $v_{1t}'$ , respectively. A detailed description of this procedure and several applications have been reported (17, 18). Important is that the primary ion beam is entering very close to the axis using a small hole in the injection electrode and with a small angular divergence by operating all lens elements at the same voltage.

Recent examples include the near symmetric charge transfer in  $^{36}\text{Ar}^+ + ^{40}\text{Ar}$  collisions (19) and the dynamically restricted scrambling in  $^{15}\text{N}^+ + ^{14}\text{N}_2$  collisions (20). Figure 14 shows axial velocity distributions measured at  $E_T = 6\text{ eV}$  for the two isotopically different charge transfer products (Eqn. (21)).

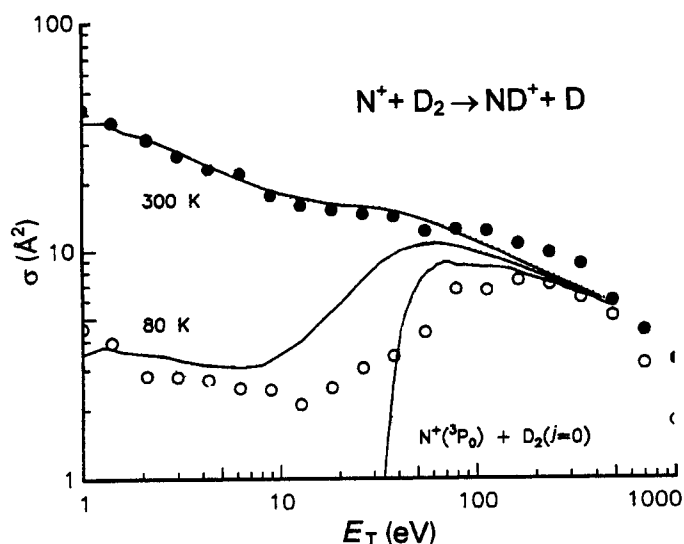
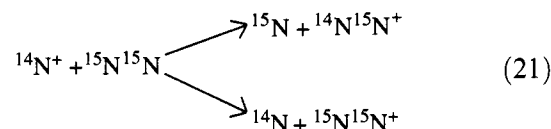


**Figure 12**

Merged beam results for the reaction  $\text{N}^+ + \text{D}_2 \rightarrow \text{ND}^+ + \text{D}$  measured for two different nozzle temperatures (80 K: open circles; 300 K: solid dots). The solid lines are calculated effective cross-sections determined from a properly weighted sum of state-specific cross-sections calculated with phase space theory. The lowest curve is the theoretical result for ground state reactants.



Formation of  $^{14}\text{N}^{15}\text{N}^+$  in an atom transfer process (upper panel) shows a preference for forward scattering, whereas for electron transfer, backward scattering prevails (lower panel). As illustrated by the open and the filled symbols, this is in qualitative accordance with a simple kinematic model.

## 7. Conclusions

Although the first GIB apparatus already demonstrated unique features from its beginning, its incorporation into other laboratories has been rather slow in the first decade of its invention. Meanwhile the technique has become accepted and,

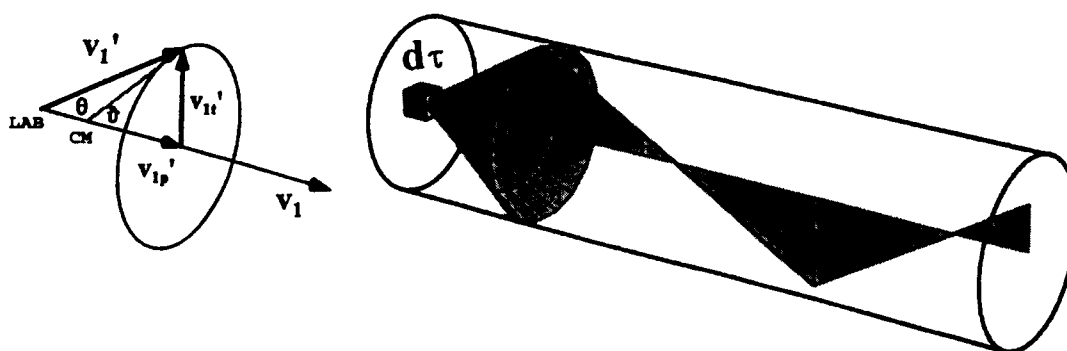


**Figure 13**

Determination of the two components  $v_{1p}'$  and  $v_{1t}'$  of the product velocity vector  $v_1'$  using the GIB method. Products starting close to the center line in the small volume  $d\tau$  are guided by the effective potential without changing their axial velocity component,  $v_{1p}'$ . The transverse velocity component,  $v_{1t}'$ , only changes sign and can be probed by variation of the effective potential.

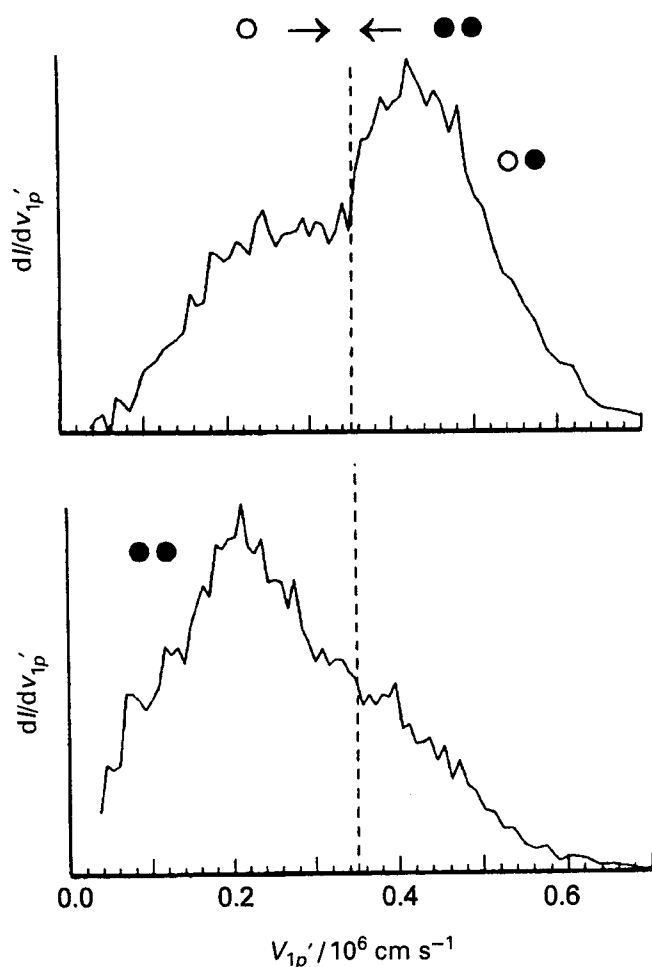


**Figure 14**

Axial product ion velocity distributions measured for two different products from  $^{14}\text{N}^+ + ^{15}\text{N}^{15}\text{N}$  at  $E_T = 6\text{ eV}$ . Formation of  $^{14}\text{N}^{15}\text{N}^+$  (upper panel) shows a preference for forward scattering, whereas electron transfer leading to  $^{15}\text{N}^{15}\text{N}^+$  backward scattering prevails (lower panel). The dashed line in the middle indicates the position of the center of mass velocity. In the center of mass frame, the  $^{14}\text{N}^+$  comes from the left (open circle), whereas the  $^{15}\text{N}^{15}\text{N}$  (closed circles) comes from the right.

worldwide, about a dozen GIB machines can be found in ion research (10). GIB machines are also commercially available. In addition, RF octopoles are used for transport, relaxation, phase space compression, chemical probing, and other applications in many modern mass spectrometers. The number of research groups routinely profiting from the advanced features of the technique are still limited to a few. This is probably because more engineering is required in order to make the sophisticated merged beam apparatus a reliable tool for routine measurements and more training is needed to establish the measuring routines for differential cross-section measurements.

All the applications mentioned in this article are based on the adiabatic approximation, used to define safe operating conditions. It may be useful for further development that more mathematical work is done for exploring more general features of the ion motion in oscillatory fields. For example, it is an open question as to whether there is any suitable RF device, besides the quadrupole, in which one could take experimental advantage of sharp transitions from stability to instability, e.g., for mass or phase-space selection. The applicability of RF devices can be further extended by superimposing additional temporal or spatial varying fields (auxiliary low-frequency field, pulsed electrodes, field penetration from correction electrodes, etc.). Also the superposition of RF and magnetic fields has been excluded so far in theory and in practice. This combination certainly could be very useful as can be seen from the versatility of FTICR instruments (see *Instrumentation: Fourier Transform Ion Cyclotron Resonance*).

The GIB technique is a versatile tool and there is no doubt that more complicated instruments will be constructed. For example, combinations with laser-based methods such as multiphoton ionization, one- or two-color fragment spectroscopy, laser-induced fluorescence, and infrared excitation of ions or neutrals will allow for many new applications in spectroscopy, reaction dynamics, analytical chemistry, and material science. Closely related to the RF ion guides are the RF traps. Confinement of charged particles in suitable fields has also become a mature field in ion chemistry (see *Instrumentation: Ion Traps*).

### Bibliography

- (1) Gerlich, D. Inhomogeneous Electrical Radio Frequency Fields: A Versatile Tool for the Study of Processes with Slow Ions. *Adv. Chem. Phys.* **1992**, *82*, 1–176.
- (2) Landau, L. D.; Lifschitz, E. M. Electrodynamics of Continuous Media. In *Theoretical Physics*; Pergamon: Oxford, UK, 1960; Vol. 1, p 93.
- (3) Mark, S.; Glenewinkel-Meyer, T.; Gerlich, D. REMPI in a Focusing Rf Quadrupole: A New Source for Mass and State Selected Ions. *Int. Rev. Phys. Chem.* **1996**, *15*, 283–298.
- (4) Dawson, P. H. *Quadrupole Mass Spectrometry and Its Applications*; Elsevier: Amsterdam, 1976.
- (5) Tatarczyk, H.; von Zahn, U. Nachweis metastabiler Ionen mit langen Lebensdauern. *Z. Naturforsch.* **1965**, *A20*, 1708.
- (6) Gerlich, D. Messungen totaler Querschnitte von Ionen-Molekül-Reaktionen bei niederen Energien. Diploma Thesis, University of Freiburg, 1971.
- (7) Henchman, M. In *Ion-Molecule Reactions*; Franklin, J. L., Ed.; Plenum: New York, 1972; Vol. 1, pp. 101–105.
- (8) Teloy, E.; Gerlich, D. Integral Cross Sections for Ion-Molecule Reactions: The Guided Beam Technique. *Chem. Phys.* **1974**, *4*, 417–427.

- (9) Anderson, S. L.; Houle, F. A.; Gerlich, D.; Lee, Y. T. The Effect of Vibration and Translational Energy on the Reaction Dynamics of the  $H_2^+ + H_2$  System. *J. Chem. Phys.* **1981**, *75*, 2153–2162.
- (10) Armentrout, P. B. Kinetic Energy Dependence of Ion–Molecule Reactions: Guided Ion Beams and Threshold Measurements. *Int. J. Mass Spectrom.* **2000**, *200*, 219–241.
- (11) Ervin, K.; Loh, S. K.; Aristov, N.; Armentrout, P. B. Metal Cluster Ions: The Bond Energy of  $Mn_2^+$ . *J. Phys. Chem.* **1983**, *87*, 3593–3596.
- (12) Hanley, L.; Anderson, S. L. Chemistry and Cooling of Transition Metal Cluster Ions. *Chem. Phys. Lett.* **1985**, *122*, 410–414.
- (13) Ng, C.-Y. State-selected and State-to-state Ion–Molecule Reaction Dynamics by Photoionization and Differential Reactivity Methods. *Adv. Chem. Phys.* **1992**, *82*, 401–500.
- (14) Guyon, P. M.; Bellec, G.; Dutuit, O.; Gerlich, D.; Gislason, E. A.; Ozenne, J. B. Use of Synchrotron Radiation to Study Ion–Molecule Reactions. *Bull. Soc. Roy. Sci. Liege*, **1989**, *58e*, 187–198.
- (15) Gerlich, D. Low Energy Reactions Measured With Guided Beams. In *Electronic and Atomic Collisions*; Lorents, D. C., Ed.; Elsevier: Amsterdam, 1986, pp 541–553.
- (16) Scherbarth, S.; Gerlich, D. Energy Partitioning in  $Ar^+ + O_2$  Collisions at Low Energies: Analysis of Product States by Laser-induced Predissociation. *J. Chem. Phys.* **1989**, *90*, 1610–1623.
- (17) Mark, S.; Gerlich, D. Differential Cross Sections, Measured with Guided Ion Beams. Applications to  $N^+ + N_2$  and  $C_2H_2^+ + C_2D_4$  Collisions. *Chem. Phys.* **1996**, *209*, 235–257.
- (18) Anderson, S. L. Mode-selective Differential Scattering as a Probe of Polyatomic Ion Reaction Mechanisms. *Acc. Chem. Res.* **1997**, *30*, 28–36.
- (19) Pullins, S.; Dressler, R. A.; Torrents, R.; Gerlich, D. Guided-ion Beam Measurements of  $Ar^+ + Ar$  Symmetric Charge-transfer Cross Sections at Ion Energies Ranging from 0.2 to 300 eV. *Z. Physik. Chem.* **2000**, *214*, 1279–1297.
- (20) Glosik, J.; Luca, A.; Mark, S.; Gerlich, D. Guided Ion Beam Studies of Electron and Isotope Transfer in  $^{14}N^+ + ^{15}N_2$  Collisions. *J. Chem. Phys.* **2000**, *112*, 7011–7021.
- (21) Muntean, F.; Armentrout, P. B. Guided Ion Beam Study of Collision-induced Dissociation Dynamics: Integral and Differential Cross Sections. *J. Chem. Phys.* **2001**, *115*, 1213–1228.
- (22) Bustamente, S. W.; Okumura, M.; Gerlich, D.; Kwok, H. S.; Carlson, L. R.; Lee, Y. T. Spin-forbidden Radiative Decay of the  $a^4P_u$  state of  $O_2^+$ . *J. Chem. Phys.* **1987**, *86*, 508–515.
- (23) Hauffler, E.; Schlemmer, S.; Gerlich, D. Absolute Integral and Differential Cross Sections for the Reactive Scattering of  $H^- + D_2$  and  $D^- + H_2$ . *J. Phys. Chem.* **1997**, *101*, 6441–6447.
- (24) Gerlich, D. Kinematic Averaging Effects in Thermal and Low Energy Ion–Molecule Collisions. *J. Chem. Phys.* **1989**, *90*, 127–139.
- (25) Tosi, P.; Dmitrijev, O.; Bassi, D.; Wick, O.; Gerlich, D. Experimental Observation of the Energy Threshold in the Ion–Molecule Reaction  $N^+ + D_2 \rightarrow ND^+ + D$ . *J. Chem. Phys.* **1994**, *100*, 4300–4307.
- (26) Gerlich, D.; Disch, R.; Scherbarth, S.  $C^+ + H_2(j) \rightarrow CH^+ + H$ . The Effect of Reagent Rotation on the Integral Cross Section in the Threshold Region. *J. Chem. Phys.* **1987**, *87*, 350–359.

D. Gerlich

Technische Universität, Chemnitz, Germany

## Ion Storage Rings

### 1. Introduction

Magnetic analyzers are widely used in mass spectrometry to separate a fast beam of ions based on the mass-to-charge ratio  $m/z$ . Several magnetic analyzers can be combined in tandem systems, and they can be combined with electrostatic analyzers to provide energy filtering. Commonly, ions pass through mass spectrometers built on magnetic and electrostatic analyzers with high speed, so that the time from ion formation to ion detection (i.e., destruction) is of the order of microseconds. In Fourier transform ion cyclotron resonance mass spectrometers (see *Instrumentation: Fourier Transform Ion Cyclotron Resonance*) ions can be trapped for a very long time in a small volume. When several magnetic or electrostatic analyzers are combined so that the ions make closed orbits while being guided by magnetic or electric fields, an ion storage ring is obtained. Ion storage rings combine the beam properties of the magnetic analyzers with the storage properties of the ion cyclotron trap.

Ion storage rings are used in particle, nuclear, atomic, molecular, and chemical physics. An advanced ion storage ring, the Large Hadron Collider (LHC), is being built at the European particle physics laboratory, CERN, in Geneva, Switzerland. However, the use or intended use of storage rings in high-energy physics is beyond the scope of this article, not least because the physics at this high-energy frontier has very little to do with mass spectrometry. The ion storage rings that have been built for atomic and molecular physics, however, have many features in common with instruments used in mass spectrometry, and, as we will see later, they are sometimes also used as mass spectrometers.

Atomic and molecular physics with ion storage rings have been reviewed several times, and the reader is referred to these reviews for a comprehensive coverage of the topic (1–5).

### 2. Experimental

Figure 1 shows the ion storage ring CRYRING at the Manne Siegbahn Laboratory, Stockholm University, Sweden. It consists of several different ion sources